PAPER

A motion planning algorithm for the feed support system of FAST

To cite this article: Rui Yao *et al* 2020 *Res. Astron. Astrophys.* **20** 068

View the article online for updates and enhancements.

A motion planning algorithm for the feed support system of FAST

Rui Yao (姚蕊), Peng Jiang (姜鹏), Jing-Hai Sun (孙京海), Dong-Jun Yu (于东俊) and Chun Sun (孙纯)

National Astronomical Observatories, Chinese Academy of Sciences, Beijing 100101, China; *pjiang@nao.cas.cn, ryao@nao.cas.cn*
CAS Key Laboratory of FAST, National Astronomical Observatories, Chinese Academy of Sciences, Beijing 100101, China

Abstract The paper relates to a motion planning algorithm for the feed support system of the Five-hundred-meter Aperture Spherical radio Telescope (FAST). To enhance the stability of the feed support system, the start/termination planning segments are adopted with an acceleration and deceleration section. The source switching planning adopts a combination of a line segment and focal segment to realize stable control of the feed support system. Besides, during the observation trajectory, a transition segment which is not used for observation data is planned with a required time. Through an example simulation, a smooth change is realized via the motion planning algorithm and presented in this paper.

Key words: FAST — radio telescope — motion planning

1 INTRODUCTION

As displayed in Figure 1, the Five-hundred-meter Aperture Spherical radio Telescope (FAST), which is the largest single-dish radio telescope in the world (Nan 2006; Nan et al. 2011), was completed with its main structure installed on 2016 September 25, after which it entered the commissioning phase (Jiang et al. 2019; Qian et al. 2019; Lu et al. 2019).

The main structures of FAST include the active reflector and the feed receiving device. The basic idea of FAST is to reflect and collect radio waves through the active reflector, which can be deformed from a spherical shape to a paraboloid with a 300 m aperture. Then, the feed receivers, which are installed in the feed support system, collect all the radio waves at the focal point of the paraboloid reflector. Figure 2 demonstrates the three active control mechanisms of the feed support system (Tang & Yao 2011): a six-cable-driven parallel robot, an A-B rotator and a Stewart parallel manipulator. The Stewart parallel manipulator is divided into upper and lower platforms. All the feed receivers are equipped on the lower platform of the Stewart manipulator. The A-B rotator and the Stewart manipulator are controlled in the feed cabin. The six-cable-driven parallel robot can maneuver the feed receivers to the correct position, but the orientation of the feed receivers cannot by itself meet the requirement for receiving the signals

(Yao et al. 2014; Li & Yao 2014), so the A-B rotator in the feed cabin is utilized to adjust the orientation of the feed to the direction on the celestial source. Through the simulation analysis of the six-cable driven parallel robot, it is found that the influence of wind disturbance is obvious. Therefore, a Stewart manipulator with six degrees of freedom is adopted to reduce the influence of wind disturbance (Shao et al. 2011, 2012), and further adjust the position and orientation of the feed receivers to acquire the radio signal with high accuracy (Yao et al. 2017).

To meet the requirements for astronomical observation, the position, velocity and acceleration of the feed support system should be planned, so as to ensure the stability and efficiency of the observation. Most of the existing motion planning methods rely on an astronomical coordinate system, which cannot guarantee the motion stability of the mechanisms in the Cartesian coordinate system. It may result in a large control error, which exceeds the accuracy requirements of feed positioning, making the observation data unavailable. Therefore, the motion planning algorithm for the feed support system of FAST needs to be improved, especially at the start and end stages, as well as the acceleration and deceleration stages during observation.

This paper introduces a new motion planning algorithm for the feed support system under the Cartesian coordinate system. Section 2 describes the feed support system and its key parameters. In Section 3, the motion planning

Fig. 1 Overview of FAST.

| (a) | (b) | (c) |
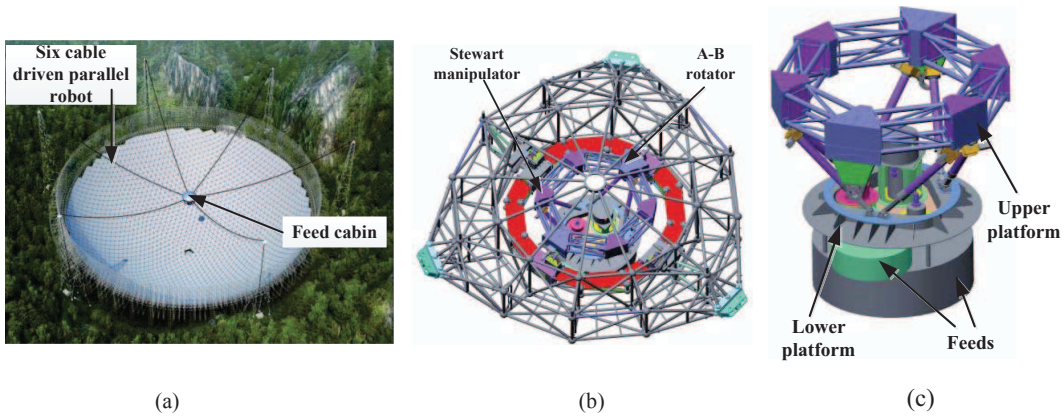
Fig. 2 Feed support system. (a) Design of the feed support system for FAST; (b) Feed cabin; (c) Stewart manipulator.

algorithm of the feed support system is presented in detail. Section 4 provides a simulation and discussion of the motion planning algorithm in this paper.

2 DESCRIPTION OF THE FEED SUPPORT SYSTEM

As illustrated in Figure 3, the feed support system mainly includes the six-cable-driven parallel robot, the A-B rotator, the Stewart manipulator and the multi-feed rotating mechanism.

In Figure 3, related coordinates are defined as: The origin point of an inertial frame $\Re : O - XYZ$ is located at the focus of the active reflector. X-axis points to the east direction, and Y-axis points to the north direction. Three cable-cabin anchoring points shape the moving plane of the six-cable driven parallel manipulator. The origin point of moving frame $\Re_C : O_C - X_C Y_C Z_C$ is located at the center of the moving plane. Initially, the moving plane of

the six-cable driven parallel manipulator is placed horizontally. In this condition, the X-axis points to the east direction and Y-axis points to the north direction. The origin point of frame $\Re_{AB} : O_{AB} - X_{AB} Y_{AB} Z_{AB}$ is located at the center of the A-B rotator. Initially, the A-B rotator is placed horizontally. In this situation, the X-axis points to the east direction and the Y-axis points to the north direction. The origin point of frame $\Re_S : O_S - X_S Y_S Z_S$ is located at the center of the moving platform of the Stewart manipulator. In this condition, the X-axis points to the east direction and Y-axis points to the north direction. All coordinates comply with the right hand rule.

The coordinates of the feeds under the inertial frame $\Re : O - XYZ$ can be described as

$$\boldsymbol{P}_{\text{feed}} = \boldsymbol{P}_{\text{AB}} + \boldsymbol{R}_C \cdot \boldsymbol{P}_{\text{AB}-\text{feed}} , \qquad (1)$$

where $\boldsymbol{P}_{\text{feed}}$ is the position vector of the $\Re_{AB}$ under the frame $\Re$. $\Re_C$ is the coordinate rotation matrix of $\Re_C$ rel-
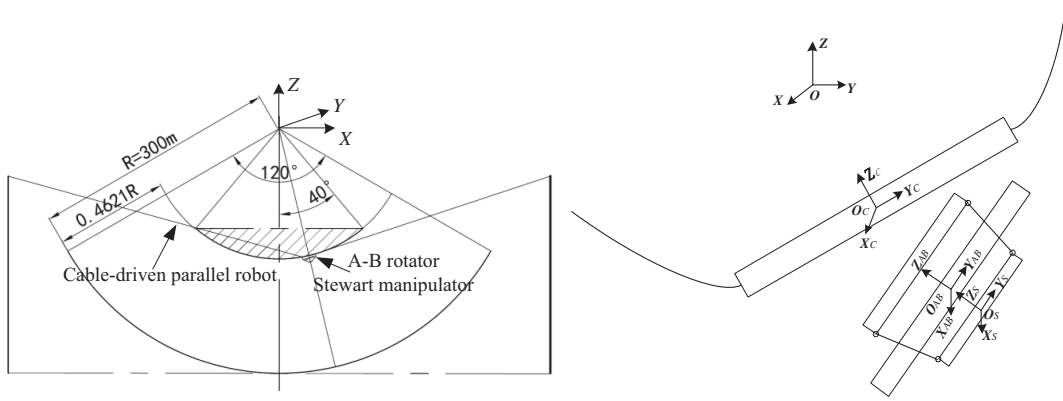
Fig. 3 Main mechanisms of the feed support system.
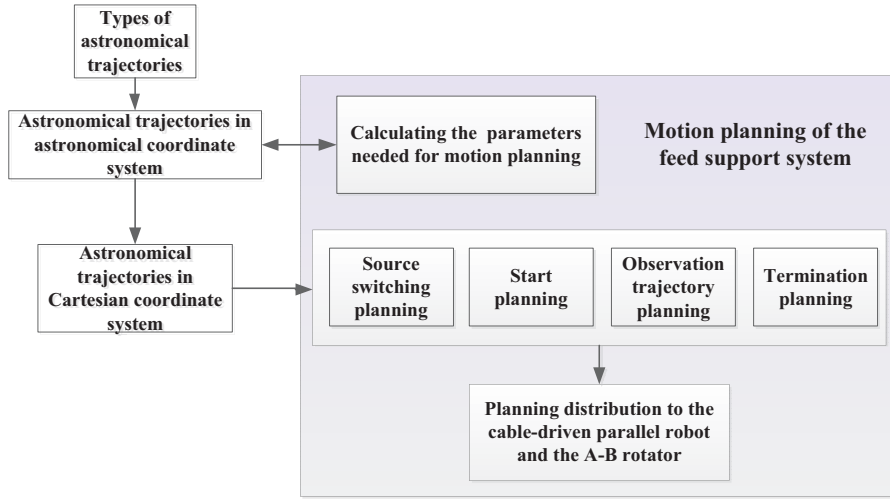
Fig. 4 Motion planning process of the feed support system.

ative to $\Re$. $\boldsymbol{P}_{\mathrm{AB}}$ is the position vector of the feed center under frame $\Re_{\mathrm{AB}}$. In this paper, Tilt-and-Torsion angle (Bonev 2002) is used to describe the coordinate-axis rotation matrix $\Re_C$, which can directly discriminate the azimuth and tilt angles. Three angles are defined: azimuth ϕ, tilt θ and torsion ω. These angles are easier to interpret geometrically and allow simple computation and representation of the 3D orientation workspace.

The rotation matrix is derived as follows

$$\boldsymbol{R}_C = R_a\left(\theta\right)R_z\left(\omega\right) = R_z\left(\phi\right)R_y\left(\theta\right)R_z\left(-\phi\right)R_z\left(\omega\right)$$
$$= \begin{bmatrix} c\phi c\theta c\left(\omega-\phi\right)-s\phi s\left(\omega-\phi\right) & -c\phi c\theta s\left(\omega-\phi\right)-s\phi c\left(\omega-\phi\right) & c\phi s\theta \\ s\phi c\theta c\left(-\phi\right)+c\phi s\left(\omega-\phi\right) & -s\phi c\theta s\left(\omega-\phi\right)-c\phi c\left(\omega-\phi\right) & s\phi c\theta \\ -s\phi c\left(\omega-\phi\right) & s\phi c\left(\omega-\phi\right) & c\theta \end{bmatrix} \tag{2}$$

where $c\left(*\right)$ and $s\left(*\right)$ correspond to the $\cos\left(*\right)$ and $\sin\left(*\right)$, respectively.

For the six-cable-driven parallel robot, the torsion ω is designed to be zero, so,

$$\boldsymbol{R}_C = \begin{bmatrix} c\phi c\theta c\left(-\phi\right)-s\phi s\left(-\phi\right) & -c\phi c\theta s\left(-\phi\right)-s\phi c\left(-\phi\right) & c\phi s\theta \\ s\phi c\theta c\left(-\phi\right)+c\phi s\left(-\phi\right) & -s\phi c\theta s\left(-\phi\right)-c\phi c\left(-\phi\right) & s\phi c\theta \\ -s\phi c\left(-\phi\right) & s\phi c\left(-\phi\right) & c\theta \end{bmatrix}. \tag{3}$$

The $\boldsymbol{P}_{\mathrm{AB-feed}}$ can be described as

$$\boldsymbol{P}_{\mathrm{AB-feed}} = \boldsymbol{R}_{\mathrm{AB}}\cdot\left(\boldsymbol{r}_{\mathrm{AB-s}}+\boldsymbol{r}_{\mathrm{s-feed}}\right), \tag{4}$$

where $\boldsymbol{R}_{\mathrm{AB}}$ is the coordinate rotation matrix of $\Re_{\mathrm{AB}}$ relative to $\Re_C$. $\boldsymbol{r}_{\mathrm{AB-s}}$ is the position vector of the $\Re_S$ in frame $\Re_{\mathrm{AB}}$. $\boldsymbol{r}_{\mathrm{s-feed}}$ is the position vector of the feeds in frame $\Re_S$.

In Equation (4), $\boldsymbol{R}_{\mathrm{AB}}$ should be decomposed into θ_{A} and θ_{B} in two rotational axes. According to the required azimuth angle ϕ_{AB} and tilt angle θ_{AB} of the A-B rotator, the relationship between them satisfies

$$\boldsymbol{R}_{\mathrm{AB}} = R_z\left(\alpha\right)R_y\left(\theta_{\mathrm{A}}\right)R_x\left(\theta_{\mathrm{B}}\right)R_z\left(\alpha\right), \tag{5}$$

$$\boldsymbol{R}_{\mathrm{AB}} = R_z\left(\phi_{\mathrm{AB}}\right)R_y\left(\theta_{\mathrm{AB}}\right)R_x\left(\theta_{\mathrm{AB}}\right)R_z\left(\omega_{\mathrm{AB}}\right), \tag{6}$$

where α is the angle between axis A and axis Y.
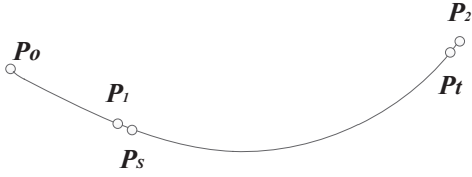
Fig. 5 A complete planning trajectory.

From Equations (5)−(6), θ_A and θ_B can be derived as

$$\sin\theta_B = \sin\alpha \cdot \cos\phi_{AB} \cdot \sin\theta_{AB} - \cos\alpha \cdot \sin\phi_{AB} \cdot \sin\theta_{AB}, \tag{7}$$

$$\sin\theta_A = \frac{\cos\alpha \cdot \cos\phi_{AB} \cdot \sin\theta_{AB} - \sin\alpha \cdot \sin\phi_{AB} \cdot \sin\theta_{AB}}{\cos\theta_B}. \tag{8}$$

From Equations (1)−(8), the position vector $\boldsymbol{P}_{AB}$, which is the control point of the cable-driven parallel robot, can be derived as

$$\boldsymbol{P}_{AB} = \boldsymbol{P}_{feed} - \boldsymbol{R}_c \cdot \boldsymbol{P}_{AB-feed}. \tag{9}$$

3 A NEW MOTION PLANNING ALGORITHM FOR THE FEED SUPPORT SYSTEM

As displayed in Figure 4, the motion planning process of the feed support system includes the following:

a) According to the types of astronomical trajectories to be observed, the time parameters needed for motion planning are calculated and sent to the astronomical trajectory planning unit.

b) According to the required observational position and time for the feeds, the motion planning of the feed support system completes the start/termination planning, the observation trajectory planning and the source switching planning.

c) Based on Equations (1)−(9), the related planning parameters of the six-cable-driven parallel robot and the A-B rotator can be calculated.

Therefore, a complete planning of the trajectories includes four parts which are depicted in Figure 5: The source switching planning trajectory

$\boldsymbol{P}_0\boldsymbol{P}_1$, the start planning trajectory $\boldsymbol{P}_1\boldsymbol{P}_s$, the observatory planning trajectory $\boldsymbol{P}_s\boldsymbol{P}_t$ and the termination planning trajectory $\boldsymbol{P}_t\boldsymbol{P}_2$.

As displayed in Figure 6, all the acceleration curves adopted in this paper are first degree curves, so that the velocity planning curves are quadratic.

3.1 Start and Termination Planning Algorithm for the Feed Support System

In order to reduce disturbance of the system due to acceleration and deceleration of the mechanisms, start and termination segments are added to buffer the disturbance and enhance the efficiency of the observatory trajectory.

According to the velocity and acceleration at the beginning of the observatory trajectory $\boldsymbol{P}_t\boldsymbol{P}_2$, the planning time and distance of the start planning trajectory can be calculated based on the given maximum velocity limit and acceleration limit of the feed support system. The coordinates $\boldsymbol{P}_1$ can be derived by the observatory trajectory on the focal surface. So, time and coordinate value planning can be calculated for the six-cable-driven parallel robot, the A-B rotator and the multi-beam rotation mechanism separately. Then, based on Equations (1)−(9), the related planning parameters of the six-cable-driven parallel robot and the A-B rotator can be calculated.

Similarly, the termination planning of the feed support system can be completed in the same way.

3.2 Source Switching Planning Algorithm for the Feed Support System

Source switching means the feed needs to move from the current position $\boldsymbol{P}_0$ to the start position $\boldsymbol{P}_1$ for the next observation task. The source switching planning can be decomposed into four steps:

a) Ascertaining $\boldsymbol{P}_h$: As shown in Figure 7, based on the geometric parameters of FAST, the closest point on the focal surface to the start position $\boldsymbol{P}_0$ can be found, which is denoted as $\boldsymbol{P}_h$. From the point $\boldsymbol{P}_0$ to the point $\boldsymbol{P}_h$, a straight line segment is used for the source switching. From the point $\boldsymbol{P}_h$ to the point $\boldsymbol{P}_1$, the focal segment is applied for source switching.

b) Calculating the source switching time: determine the source switching time for each stage of the feed support system, including the source switching time of the straight line segment (T_{focal}) and the focal segment (T_{focal}).

T_{focal}: The coordinate values of the inflection point $\boldsymbol{P}_h$ are given in Step a). Thus, the vector $\boldsymbol{P}_h\boldsymbol{P}_a$ is obtained. By setting up a maximum velocity and acceleration of the source switching trajectory, and utilizing the acceleration planning curve in Figure 6, the T_{focal} can be calculated.

T_{time}: The T_{line} is chosen as the maximum time of the source switching time for the three mechanisms and the feed position of the feed support system on the straight line segment. The three mechanisms include a six-cable-driven parallel robot, the A-B rotator and the multi-feed rotational mechanism.
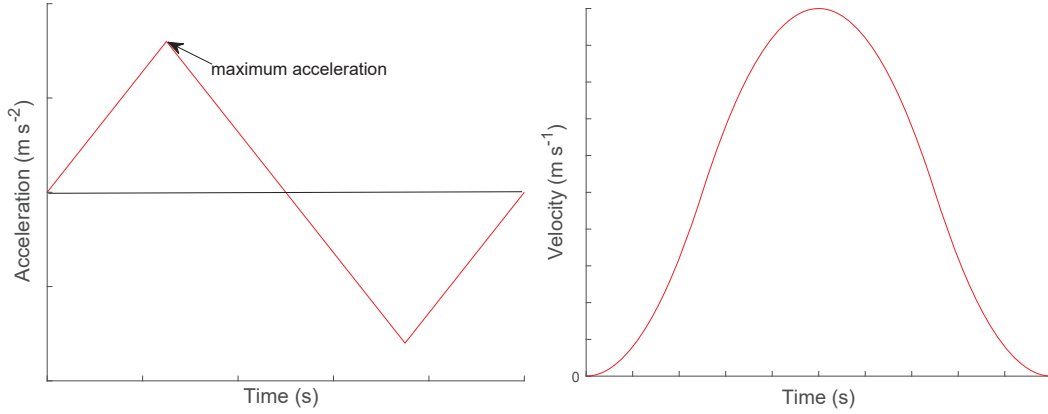
Fig. 6 Acceleration and velocity planning curves.
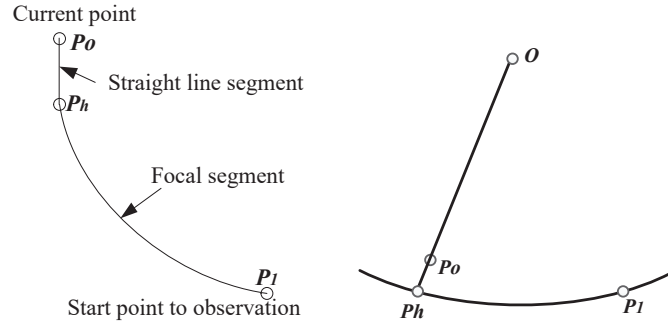
Fig. 7 A sketch map of the source switching trajectory.
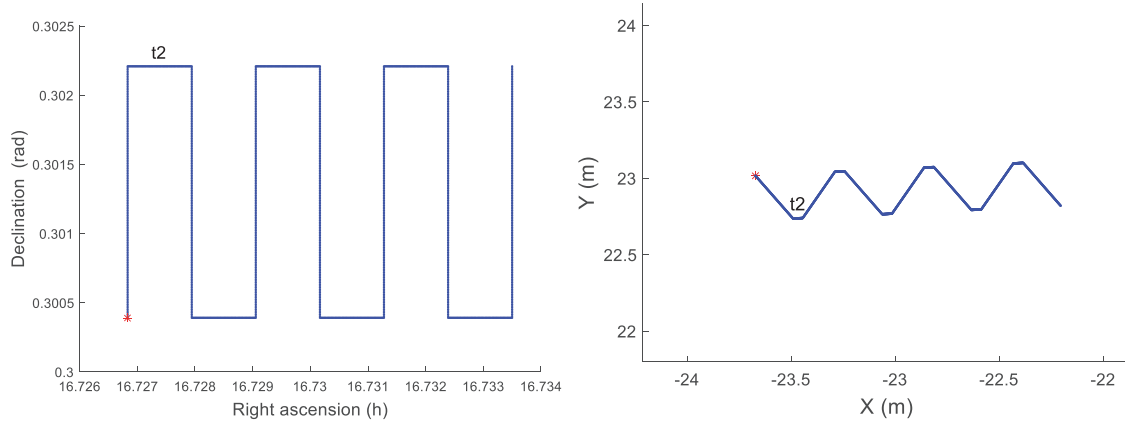
Fig. 8 A sample observation trajectory along the right ascension direction.

$$T_{\text{line}} = \max \left(T_{p-\text{line}}, T_{\text{cable}-\text{line}}, T_{\text{AB}-\text{line}}, T_{\text{multifeed}-\text{line}} \right) . \tag{10}$$

The four kinds of source switching times are calculated as follows: $T_{p-\text{line}}$ is the source switching time of the feed position on the straight line segment, which is calculated by the coordinate values of the start point P_0 and the inflection point P_h based on a given maximum velocity limit and the acceleration limit of the feed support system.

$T_{\text{cable}-\text{line}}$ is the source switching time of the angle of the cable-driven parallel robot on the straight line segment, which can be calculated by the given maximum angular acceleration and the angular velocity limit. That is to say, considering the influence of the angle of the cable-driven parallel robot on the cable force, the stability of the feed support system mechanism can be further ensured.

$T_{\text{AB}-\text{line}}$ is the source switching time of the A-B rotator on the straight line segment. According to the angle switching value of the A-B rotator and the maximum an-
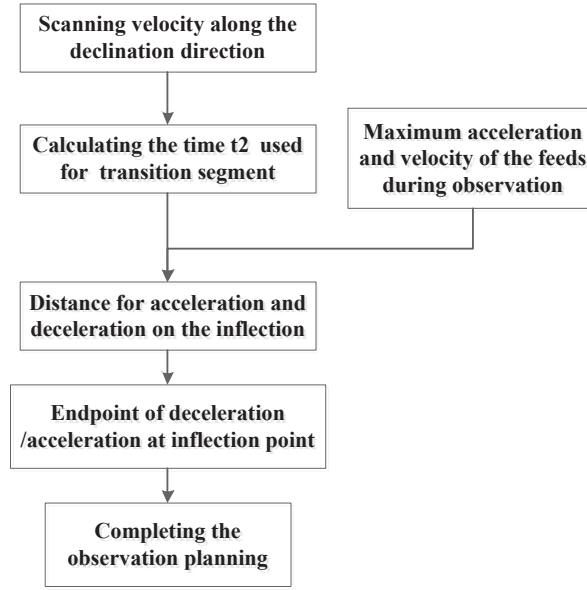
Fig. 9 Motion planning process of the motion scan along the right ascension direction.
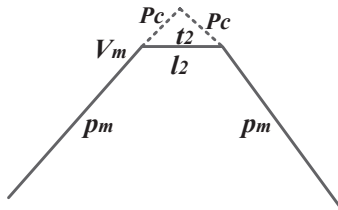
Fig. 10 Parameters related to t_2 in the Cartesian coordinate system.

gular acceleration and the angular velocity limit, the whole switching time of the A-B rotator is obtain as T_{AB}. Thus, $T_{\mathrm{AB-line}} = T_{\mathrm{AB}} - T_{\mathrm{focal}}$.

One of the feeds of FAST is the multi-feed receiver (19-beam $1.05-1.45$ GHz receiver). A rotational mechanism is installed with the multi-feed receiver to realize the rotation motion according to the requirement for astronomical observation. Similarly, the $T_{\mathrm{multifeed-line}}$ which is the source switching time of the multi-feed rotational mechanism on the straight line segment can be calculated as $T_{\mathrm{AB-line}}$.

c) Completing the source switching planning: According to the relationship between time and velocity (angular velocity) and acceleration (angular acceleration), time and coordinate value planning can be performed for the six-cable-driven parallel robot, the A-B rotator and the multi-beam rotation mechanism separately.

d) Based on Equations (1)−(9), the related planning parameters of the six-cable-driven parallel robot and the A-B rotator can be calculated.

3.3 The Observatory Planning Algorithm for the Feed Support System

The observation mode of FAST includes but is not limited to the tracking scan, drift scan, basketweave scan and motion scan. During the observation trajectory, adding acceleration and deceleration planning at the inflection point in the motion planning algorithm can ensure the motion stability and accuracy of the feed support system, which will enhance the efficiency of the observation. This paper describes the motion planning algorithm of the motion scan along the right ascension direction and the motion scan along the declination direction.

Figure 8 depicts a sample observation trajectory of the motion scan along the right ascension direction in the astronomical coordinate system and in the Cartesian coordinate system, which includes an observation segment along the declination direction (vertical line) and transition segment along the right ascension direction (horizontal line). The inflection is formed at the junction of the observation section and transition section. The data on the transition segment are not useful, thus the transition segment can be planned. For reducing the disturbance of the mechanism at the inflection, an acceleration section and a deceleration section can be added on the transition segment. Figure 9 illustrates the motion planning process. The planned time of the transition segment is defined as t_2, which is the most important parameter in the observatory planning algorithm.

Figure 10 displays the parameters related to t_2 in the Cartesian coordinate system. The dotted line is the actual route in time t_2. V_m is the velocity at the end of the ob-
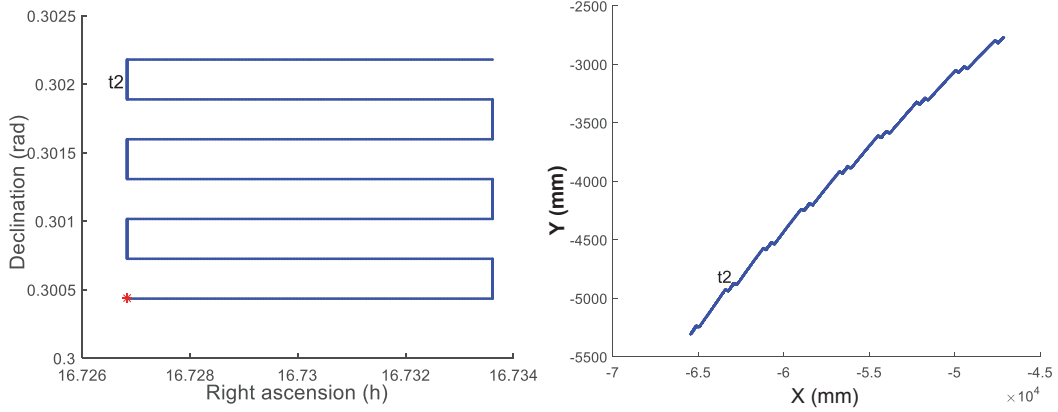
Fig. 11 A sample observation trajectory along the declination direction.
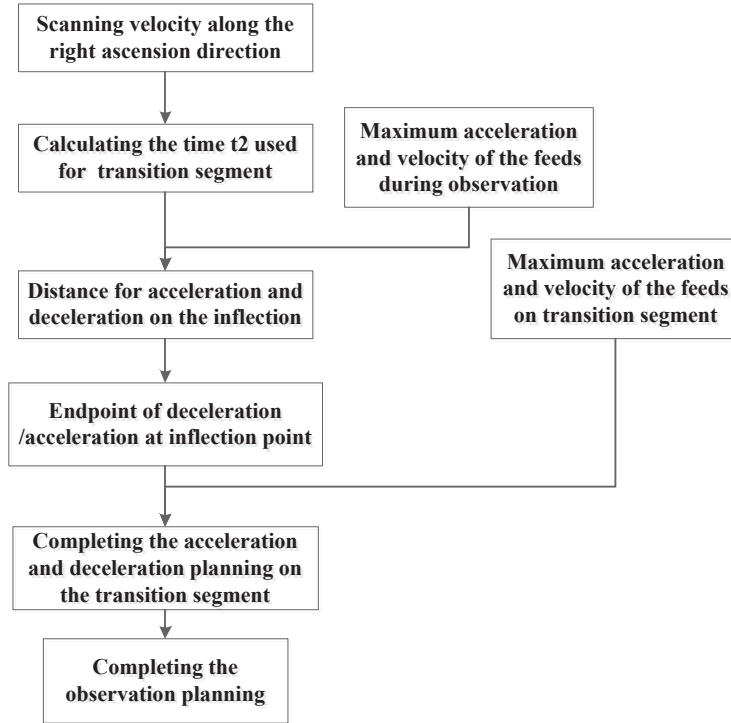
Fig. 12 Motion planning process of the motion scan along the declination direction.

servation segment (also at beginning of the transition segment), p_m is the slope of observation curve and p_c is the slope of the transition segment. Based on the analysis of the observation curve, V_m, p_m, V_c and l_2 can be described as:

$$V_m = 0.008V_{\text{dec}}^2 + 0.292V_{\text{dec}} + 10.19\,, \quad (11)$$

$$p_m = 0.079V_{\text{dec}} - 0.0133\,, \quad (12)$$

$$V_c = -0.71\frac{60}{t_2} + 10.68\,, \quad (13)$$

$$l_2 = 0.5t_2V_c\,. \quad (14)$$

Here the unit of V_m is mm s^{-1}; V_{dec} is the scanning speed in the declination direction in the astronomical coordinate system and its unit is $^\circ\,h^{-1}$; V_c is the scanning speed in the right ascension direction in the Cartesian coordinate system.

The maximum tolerance of $|p_m - p_c|$ and the maximum acceleration A_{max} can be regarded as the limiting condition to calculate t_2 by examining the acceleration curve which is shown in Figure 6.

In Figure 11, a sample observation trajectory of the motion scan along the declination direction in the astronomical coordinate system and Cartesian coordinate system includes the observation segment along the right ascension direction (horizontal line) and transition segment along the declination direction (vertical line).

Table 1 Parameters of the Feed Support System

Parameter	Symbol	Value
Radius of the reflector	R	300 (m)
Focal ratio	f	0.4621
Radius of the focal surface	r	162.15 (m)
Zenith angle	ZA	40 (°)
Maximum acceleration of the feeds on start/termination/observation planning	$A_{\max}$	10 (mm s^{-2})
Maximum acceleration of the feeds on transition segment	$A_{t-\max}$	15 (mm s^{-2})
Maximum source switching velocity of the feeds	$V_{s-\max}$	400 (mm s^{-1})
Maximum source switching acceleration of the feeds	$A_{s-\max}$	25 (mm s^{-2})
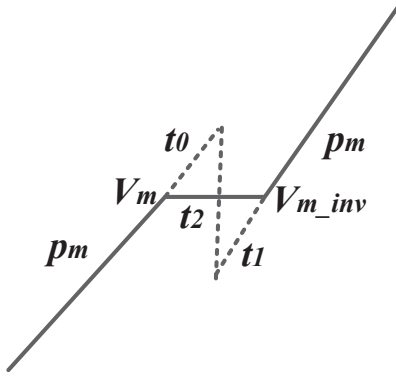
Fig. 13 Related parameters of t_2 in the Cartesian coordinate system.
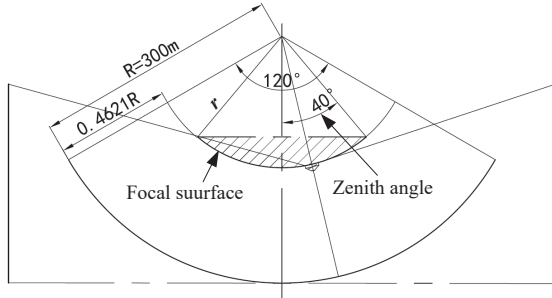
Fig. 14 A sketch map of the feed support system.

As exhibited in Figure 12, the process of motion planning for the motion scan along the declination direction is proposed, which adopts two acceleration sections and two deceleration sections on the transition segment. The planned time of the transition segment is defined as t_2, which is the most important parameter for the observatory planning algorithm.

Figure 13 shows the related parameters of the t_2 in the Cartesian coordinate system. The dotted line part is the actual route in the time t_2. V_m is the velocity at the end of the observation segment (forward direction along right ascension), and $V_{m-\mathrm{inv}}$ is the velocity at the beginning of the next observation segment (reverse direction along right ascension). Based on analysis of the observation curve, they can be described as:

$$V_m = -0.751 V_{\mathrm{asc}} + 11.3\,, \qquad (15)$$

$$V_{m-\mathrm{inv}} = 0.751 V_{\mathrm{asc}} + 11.3\,. \qquad (16)$$

Here the unit of V_m and $V_{m-\mathrm{inv}}$ is mm s^{-1}; V_{asc} is the scanning speed in the declination direction in the astronomical coordinate system and its unit is h s^{-1}.

So,

$$t_3 = t_0 + t_1 = 2V_m/A_{\max} + 2V_{m-\mathrm{inv}}/A_{\max}\,. \qquad (17)$$

Then, the scanning speed in the declination direction in the astronomical coordinate system and the Cartesian coordinate system can be described as

$$V_{\mathrm{dec}} = 60/t_3\,, \qquad (18)$$

$$V_D = 0.008 V_{\mathrm{dec}}^2 + 0.292 V_{\mathrm{dec}} + 10.19\,. \qquad (19)$$

Therefore,

$$t_2 = \frac{(2A_{\mathrm{Smax}}t_3 + 8V_D) + \sqrt{(2A_{\mathrm{Smax}}t_3 + 8V_D)^2 - 4(A_{\mathrm{Smax}}t_3)^2}}{2A_{\mathrm{Smax}}}\,. \qquad (20)$$

4 SIMULATION AND DISCUSSION

The main parameters of the feed support system are displayed and listed in Figure 14 and Table 1.

As an example, motion scan trajectories along the right ascension direction are planned as depicted in Figure 15.

Then, the velocity and acceleration result of this trajectory with start and termination planning is shown in Figure 16.

According to Figure 16, the motion planning algorithm ensures the moving velocity of the feed support system is consistent with the observation speed on the observation segment. Meanwhile, the lower change rate of the velocity and the acceleration of the feed support system reduce the disturbance of the mechanisms, leading to a stability feed support system and a high observation efficiency. Then, planning for the source switching can be completed based on P_0 and P_1, and the Figure 17 demonstrates the one cable planning result of the six-cable driven parallel manipulator, which is stable.
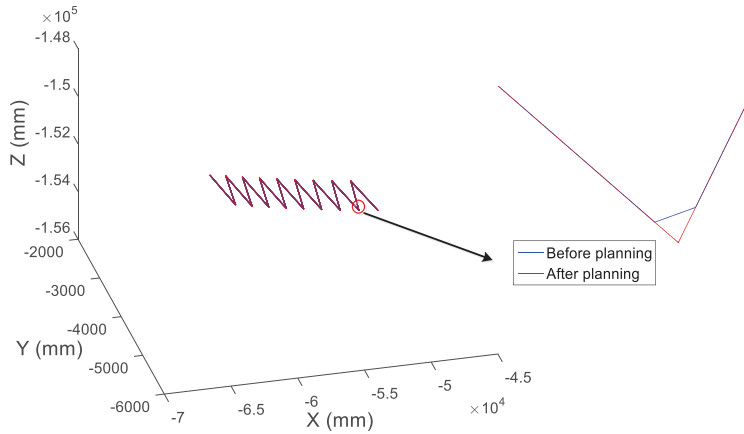
Fig. 15 Motion scan trajectories along the right ascension direction.
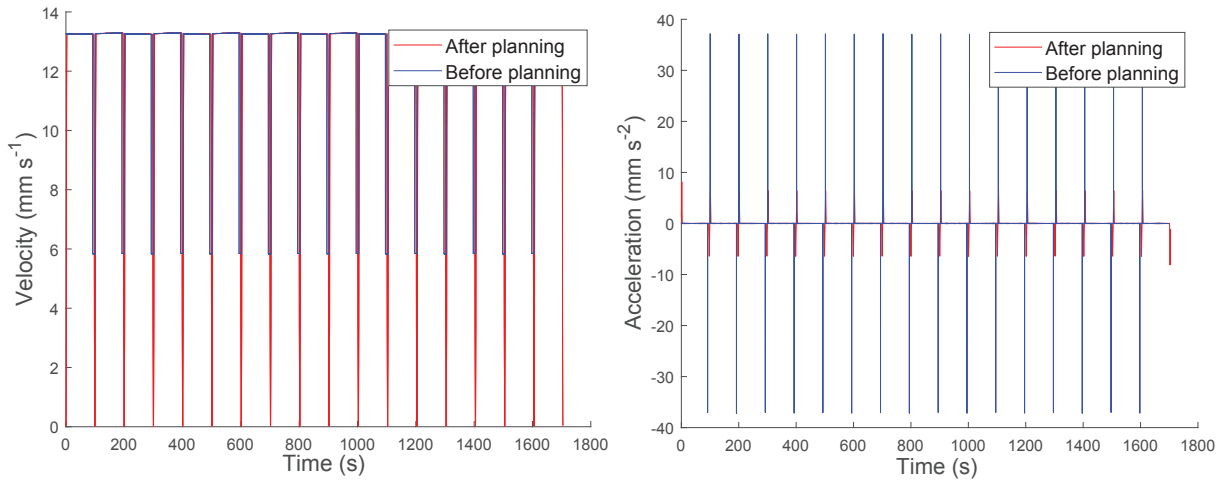
Fig. 16 A motion planning result of a motion scan trajectory along the right ascension direction with start and termination planning. *Left:* The velocity of the trajectory; *Right:* The acceleration of the trajectory.
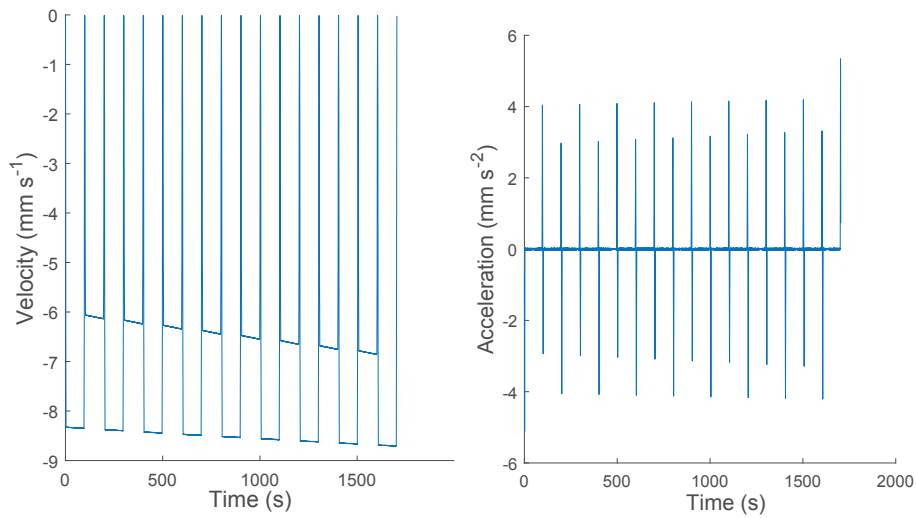
Fig. 17 A motion planning result for the cable driven parallel robot. *Left:* The velocity of the trajectory; *Right:* The acceleration of the trajectory.

5 CONCLUSIONS

This paper presents a motion planning algorithm for the feed support system. Firstly, start/termination planning is adopted for reducing the mechanism disturbance at the beginning/termination of the observation. Secondly, in the process of source switching, a combination of the line segment and focal segment is adopted to reduce the change in force of the six-cable-driven parallel robot, which can control stability of the feed support system. Thirdly, a transition segment with planned time is used for reducing the control error on the inflection point of the observation trajectory, which can enhance the observation data efficiency. Finally, a simulation indicates the smooth change by the motion planning algorithm implemented in this paper.

References

Bonev, I. A. 2002, Geometric Analysis of Parallel Mechanisms, PhD Thesis, Laval University, Canada

Jiang, P., Yue, Y., Gan, H., et al. 2019, Science China Physics, Mechanics, and Astronomy, 62, 959502

Li, H., & Yao, R. 2014, Advances in Mechanical Engineering, 2014, 716097

Lu, J., Peng, B., Liu, K., et al. 2019, Science China Physics, Mechanics, and Astronomy, 62, 959503

Nan, R. 2006, Science in China: Physics, Mechanics and Astronomy, 49, 129

Nan, R., Li, D., Jin, C., et al. 2011, International Journal of Modern Physics D, 20, 989

Qian, L., Pan, Z., Li, D., et al. 2019, Science China Physics, Mechanics, and Astronomy, 62, 959508

Shao, Z. F., Chen, X., Wang, L., & Tang, X. 2011, Robotica, 29, 903

Shao, Z. F., Tang, X., Chen, X., & Wang, L. P. 2012, Robotics and Computer Integrated Manufacturing, 28, 649

Tang, X., & Yao, R. 2011, Journal of Mechanical Design, 133, 111012

Yao, R., Zhu, W., Sun, C., Li, H., & Sun, J. 2014, Advances in Mechanical Engineering, 2014

Yao, R., et al. 2017, Journal of Mechanical Engineering, 17, 36